IET Optoelectronics

Research Article

IET Journals
The Institution of Engineering and Technology

Design of optical fibre coaxial couplers with arbitrary modal electric field

ISSN 1751-8768
Received on 25th November 2018
Revised 2nd October 2019
Accepted on 22nd October 2019
E-First on 28th January 2020
doi: 10.1049/iet-opt.2018.5155
www.ietdl.org

Konstantinos Aidinis[1] ✉, *Kostas Angelis*[2], *Anthony Boucouvalas*[2]

[1]*Electrical Engineering, Ajman University, P.O. Box 436, Ajman, UAE*

[2]*Informatics and Telecommunications, University of Peloponnese, Tripoli 22100, Greece*

✉ *E-mail: k.aidinis@ajman.ac.ae*

Abstract: The authors analyse a method, which leads to an efficient and precise algorithm for synthesising coaxial, optical fibre couplers of arbitrary modal electric-field distributions. Their purpose is to design a fibre optic index profile supporting two pre-selected mode fields such that their interference transfers all the optical power spatially from the core region to a cladding part of the optical fibre completely. To deal with this problem, they apply inverse transmission-line techniques. Using the desired electric field, they work inversely and synthesise the appropriate refractive index profile of the couplers with excellent crosstalk. They envisage one can apply this technique to design fibre optic coaxial components acting as filters in sensing and numerous other applications.

Nomenclature

c	speed of light in vacuum
I_E	electric current
I_M	magnetic current
k_0	free space propagation constant
K	modified Bessel function
l	azimuthal mode number
L	beat length
n	refractive index
V_E	electric voltage
V_M	magnetic voltage
Z_0	free space impedance
β	wave propagation constant
$\overline{\beta}$	normalised β
ε	electric permittivity
λ	optical wavelength
μ_r	relative permeability
μ_0	permeability of free space
σ	conductivity, standard deviation
ω	angular frequency

1 Introduction

Traditionally, the study of two waveguides forming an optical fibre coupler has normally been carried out by calculating the coupling coefficient between them. The use of perturbation theory combined with knowledge of the optical fields and propagation constants of the modes of the separate waveguides is normally sufficient to work out the optical power transfer between them. Phase matching between the fundamental modes of the two separate waveguides is necessary to have complete power transfer between the two coupled waveguides. Alternatively, if one could determine the propagation constants and mode field intensity of the modes of the combined structure, then interference between the modes involved can offer the optical power re-distribution within the combined structure of the coupler [1]. There have been numerous research efforts in determining the optical properties of couplers, but usually, the devices are being made from step-index optical fibres. Coaxial couplers, the combination of a step-index core waveguide, and a step-index tubular waveguide surrounding this [2] have been studied and shown to be very interesting for filter design, sensing and modulator applications [3–6]. Since the study of all fibre–coaxial coupler devices so far has been using mainly based on the use of step-index waveguides, where the modal fields follow Bessel functions. If the desired modal field shape of the surrounding waveguide is not desired to be of Bessel shape, there is no available technique to allow the design of such components. It is desirable as a starting point to be able to use the two-mode interfering fields to be of suitably arbitrary shapes, which facilitate the application to be had, and from those modes to be able to design coaxial coupler index profile, which supports the desired modal fields. We show that this method can offer excellent coupler crosstalk designs. Our purpose is to design a fibre optic device with two pre-selected mode fields such that the beating of those two fields transfers all the optical power in one or the other part of the optical fibre. As an example of a step-index fibre, the profile is the coaxial coupler [2]. This is an optical fibre, which can be seen as the sum or combination of a step-index core (rod) and a tubular waveguide (tube). The combined structure can be seen as a coaxial coupler (Fig. 1) alternatively; one can view this refractive index (RI) profile as a single combined multimode fibre, rather than two coupled waveguides. Applications of such a device are, for example, in optical filtering, sensing and modulators. Our fundamental problem apart from designing such components is the design of fibres from knowledge of the sum and difference of their electric fields. The beating (sum and difference) of the fields would shift periodically the optical energy in the core or selected ring in the cladding along the propagation length. The novelty in this case is the ability to design such waveguides, which are not restricted to have only Bessel function modal field distributions but to have the flexibility of other desirable shapes, especially in regions within the waveguide such as the cladding, where one may wish to have better control of the field distribution. The reconstructed waveguide supporting this idea will not be necessary of the well known rod in tube profiles. As a coupler, this general waveguide can be designed to work as an optical filter or sensor as demonstrated in the references for step-index profile [7–10], while selecting a desired modal field distribution enables us to combine additional features such as the choice of a flattened electric field that is useful for high-power laser or amplifier applications. Also, we have the ability to design optical fibres with desired modal field distributions for two rather than one mode under the condition of coupling.

The basic theory alongside with results and conclusions is provided in the following sections.

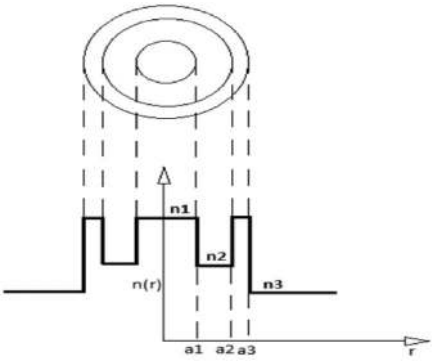

Fig. 1 *Index distribution in the step-index coaxial coupler*

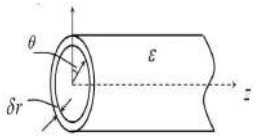

Fig. 2 *Homogeneous optical fibre thin cylindrical layer*

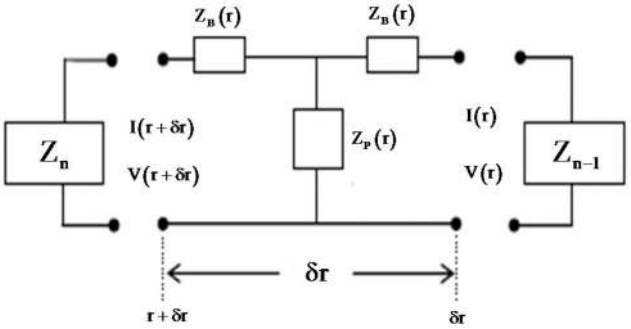

Fig. 3 *Equivalent circuit for an optical fibre cylindrical thin layer*

2 Transmission-line (T–L) theory description

According to our modelling, a cylindrical optical fibre is split into a sufficient number of concentric homogeneous cylindrical layers of thickness δr, conductivity σ, permittivity ε and permeability μ in Fig. 2.

Maxwell's equations for the E and H fields are applied to each such layer [11]

$$\left.\begin{aligned} \beta r E_\theta - l E_z &= \omega\mu r H_\mathrm{r} \\ l H_z - \beta r H_\theta &= (\omega\varepsilon - \mathrm{j}\sigma) r E_\mathrm{r} \\ \frac{\partial(\omega\mu r H_\mathrm{r})}{\partial r} &= -\mathrm{j}\omega\mu(l H_\theta + \beta r H_z) \end{aligned}\right\} \tag{1}$$

$$\left.\begin{aligned} \frac{\partial(\omega\varepsilon - \mathrm{j}\sigma) r E_\mathrm{r}}{\partial r} &= -(\sigma + \mathrm{j}\omega\varepsilon)(l E_\theta + \beta r E_z) \\ \frac{\partial(l H_\theta + \beta r H_z)}{\partial r} &= \mathrm{j}\gamma_{\mathrm{s,\,d}}^2 r H_\mathrm{r} + \beta H_z - \frac{l}{r} H_\theta \\ \frac{\partial(l E_\theta + \beta r E_z)}{\partial r} &= \mathrm{j}\gamma_{\mathrm{s,\,d}}^2 r E_\mathrm{r} + \beta E_z - \frac{l}{r} E_\theta \end{aligned}\right\} \tag{2}$$

After some algebra similar to [11, 12], (1) and (2) can be transformed into

$$\left.\begin{aligned} \frac{\partial V_\mathrm{s}}{\partial r} &= \frac{-\gamma_\mathrm{s}^2}{\mathrm{j}\omega\varepsilon_0 n F} I_\mathrm{s} \\ \frac{\partial I_\mathrm{s}}{\partial r} &= -\mathrm{j}\omega\varepsilon_0 n F V_\mathrm{s} \end{aligned}\right\} \tag{3}$$

$$\left.\begin{aligned} \frac{\partial V_\mathrm{d}}{\partial r} &= \frac{-\gamma_\mathrm{d}^2}{\mathrm{j}\omega\varepsilon_0 n F} I_\mathrm{d} \\ \frac{\partial I_\mathrm{d}}{\partial r} &= -\mathrm{j}\omega\varepsilon_0 n F V_\mathrm{d} \end{aligned}\right\} \tag{4}$$

where $\gamma_{\mathrm{s,\,d}}^2 = \beta^2 + (l/r)^2 - n^2 k_0^2 \pm \left(2n\beta l k_0/\left((\beta r)^2 + l^2\right)\right)$ (− for HE and + for EH modes) and k_0 is the free space propagation constant. Equations (3) and (4) represent two independent T–Ls with voltages V_s, V_d and currents I_s, I_d.

The following variable voltages and currents were defined:

$$\left.\begin{aligned} V_\mathrm{s} &= \frac{V_\mathrm{M}}{\sqrt{n}} + V_\mathrm{E}\sqrt{n} \quad \text{(sum)} \\ V_\mathrm{d} &= \frac{V_\mathrm{M}}{\sqrt{n}} - V_\mathrm{E}\sqrt{n} \quad \text{(difference)} \\ I_\mathrm{s} &= I_\mathrm{M}\sqrt{n} + \frac{I_\mathrm{E}}{\sqrt{n}} \quad \text{(sum)} \\ I_\mathrm{d} &= I_\mathrm{M}\sqrt{n} - \frac{I_\mathrm{E}}{\sqrt{n}} \quad \text{(difference)} \end{aligned}\right\} \tag{5}$$

and $V_\mathrm{M} = ((l H_\theta + \beta r H_Z)/\mathrm{j}F) Z_0$(magnetic voltage),
$I_\mathrm{M} = \omega\mu r H_\mathrm{r}/\mathrm{j}Z_0$(magnetic current),
$V_\mathrm{E} = ((l E_\theta + \beta r E_Z)/F) Z_0$(electric voltage),
$I_\mathrm{E} = \omega\varepsilon_0 n^2 r E_\mathrm{r}$(electric current),
$Z_0 = 120\pi$ is the free space impedance and $F = \left(\left((\beta r)^2 + l^2\right)/r\right)$.

The corresponding characteristic impedances are

$$\left.\begin{aligned} Z_\mathrm{s} &= \frac{\gamma_\mathrm{s}}{\mathrm{j}\omega\varepsilon_0 n F} \\ Z_\mathrm{d} &= \frac{\gamma_\mathrm{d}}{\mathrm{j}\omega\varepsilon_0 n F} \end{aligned}\right\} \tag{6}$$

The above equations are recognised as the well known T–L equations with the solution represented by the following electric circuit Fig. 3:

$$\left.\begin{aligned} Z_\mathrm{B} &= Z_{\mathrm{s,\,d}} \tanh\left(\gamma_{\mathrm{s,\,d}} \frac{\delta r}{2}\right) \\ Z_\mathrm{P} &= \frac{Z_{\mathrm{s,\,d}}}{\sinh(\gamma_{\mathrm{s,\,d}} \delta r)} \end{aligned}\right\} \tag{7}$$

where δr is the length of the T–L.

Since δr is infinitesimal, $\delta r/r << 1$, hence

$$\left.\begin{aligned} Z_\mathrm{B} &= \frac{1}{2}(\delta r)^2 \gamma_{\mathrm{s,\,d}}^2 Z_\mathrm{P} \\ Z_\mathrm{P} &= \frac{Z_0}{\mathrm{j}nr\delta r k_0(\beta^2 + (l/r)^2)} \end{aligned}\right\} \tag{8}$$

An optical fibre can be expressed by a sequence of T–L circuits connected in tandem. If we desire to have the optical energy trapped inside the fibre, the total impedance has to equal to zero ($Z_\mathrm{total} = 0$). On this condition, the total circuit resonates, and we can calculate the mode propagation constants using any root searching method [12].

The total impedance is expressed as the sum of Z_in and Z_out, $Z_\mathrm{total} = Z_\mathrm{in} + Z_\mathrm{out}$, where Z_in is the total impedance from up to the core-cladding boundary and Z_out the total impedance to that boundary starting from large r ($r = \infty$) in the cladding

$$Z_n = \frac{(Z_{n-1} + Z_{\mathrm{B},\,n}) Z_{\mathrm{P},\,n}}{Z_{n-1} + Z_{\mathrm{B},\,n} + Z_{\mathrm{P},\,n}} + Z_{\mathrm{B},\,n} \quad (n = 1, 2, \ldots, N) \tag{9}$$

where $Z_{\mathrm{P},\,n}$, $Z_{\mathrm{B},\,n}$ are the parallel and series elements of the T-circuit representation of the nth layer and N the number of layers.

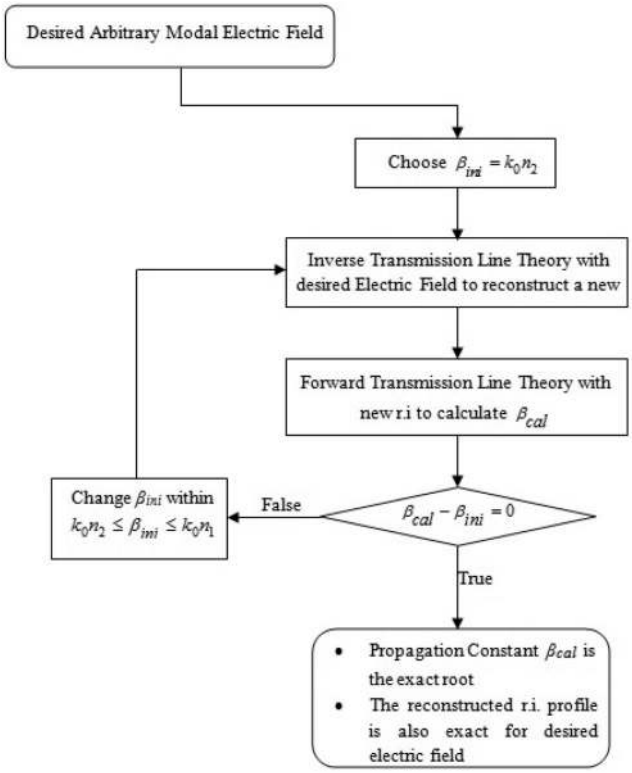

Fig. 4 *Flow diagram for calculating the exact propagation constant*

By using the propagation constant β, the mode electric field E_r can be worked out [11, 13]. From (5), the electric current I and electric field E_r can be derived

$$\left.\begin{aligned} V_{HE} &= \frac{V_M}{\sqrt{n(r)}} + V_E\sqrt{n(r)} \\ V_{EH} &= \frac{V_M}{\sqrt{n(r)}} - V_E\sqrt{n(r)} \end{aligned}\right\} \tag{10}$$

$$\left.\begin{aligned} I_{HE} &= I_M\sqrt{n(r)} + \frac{I_E}{\sqrt{n(r)}} \\ I_{EH} &= I_M\sqrt{n(r)} - \frac{I_E}{\sqrt{n(r)}} \end{aligned}\right\} \tag{11}$$

The E/M field of the HE mode in terms of the variables I_{HE} and V_{HE} will be determined; one can set $V_{HE} = I_{HE} = 0$ when the HE modes are of interest. This implies that

$$\left.\begin{aligned} I_M\sqrt{n(r)} &= \frac{I_E}{\sqrt{n(r)}} \\ \frac{V_M}{\sqrt{n(r)}} &= V_E\sqrt{n(r)} \end{aligned}\right\} \tag{12}$$

Substituting into (10) and (11), the following equations can be derived:

$$\left.\begin{aligned} V_{HE} = 2V_E\sqrt{n(r)}\,, \quad I_{HE} = 2V_M\sqrt{n(r)} \\ V_{HE} = \frac{2V_M}{\sqrt{n(r)}}\,, \quad I_{HE} = \frac{2I_E}{\sqrt{n(r)}} \end{aligned}\right\} \tag{13}$$

Note that I_{HE}, V_{HE} are also referred to as I_s, V_s, respectively

$$\left.\begin{aligned} V_E = \frac{V_s}{2\sqrt{n(r)}}\,, \quad I_M = \frac{I_s}{2\sqrt{n(r)}} \\ V_M = \frac{V_s\sqrt{n(r)}}{2}\,, \quad I_E = \frac{I_s\sqrt{n(r)}}{2} \\ I_E = \omega\varepsilon_0 n^2(r) r E_r \end{aligned}\right\} \tag{14}$$

Hence, with knowledge of $n(r)$, we can derive E_r precisely

$$E_r = \frac{I_E}{\omega\varepsilon_0 n^2(r) r} = \frac{Z_0 I_s}{2k_0 n^{3/2}(r) r} \tag{15}$$

3 Inverse problem

One of the advantages of the T–L method is that the derivation of the RI profile is possible from the knowledge of a given mode electric field.

Since electric field E_r and current I_s are known, the optical fibre RI $n(r)$ can be calculated directly from (13) as

$$n(r) = \left(\frac{Z_0 I_s}{2k_0 r E_r}\right)^{2/3} \tag{16}$$

where I_s can be recursively calculated, similarly to (7), by the following equation:

$$I_n = I_{n-1}\left(1 + \frac{Z_{n-1} + Z_{B,n}}{Z_{P,n}}\right) \quad (n = 1, 2, \ldots, N) \tag{17}$$

and

$$\lim_{n \to N} I_n = \lim_{n \to N} Z_n = 0 \tag{18}$$

for a large value of N (theoretically, $N \to \infty$).

To calculate (16), it is necessary to determine the unknown mode propagation constant β to build up the $n(r)$.

For this reason, we use the following recursive process [14], illustrated in Fig. 4. We vary β (starting with $\beta_{ini} = k_0 n_2$) within some reasonable bounds: $k_0 n_2 \le \beta_{ini} \le k_0 n_1$, and for every β_{ini} we

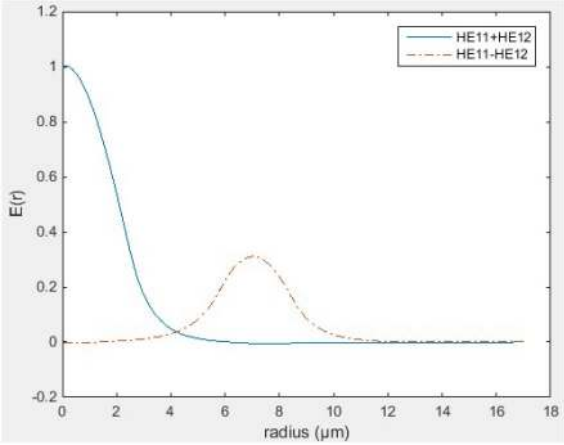

Fig. 5 *Desired power distribution of coupler in the two states, when all power in core or when all power in the cladding. The distribution corresponds to the sum and difference of HE11 and HE12 coupler modes used for the mode field synthesis of the optical, coaxial coupler*

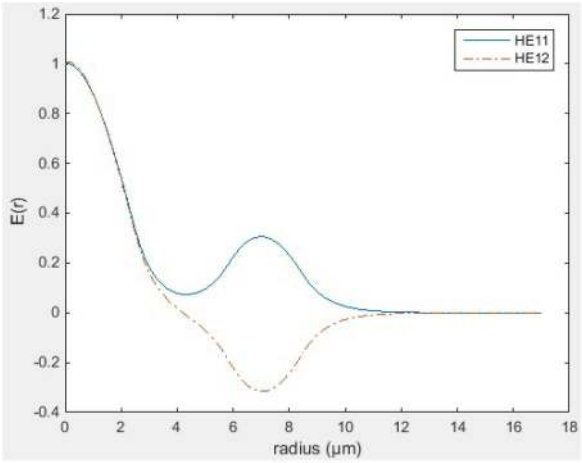

Fig. 6 *Derived HE11 and HE12 modes versus the radius (from fields in Fig. 5)*

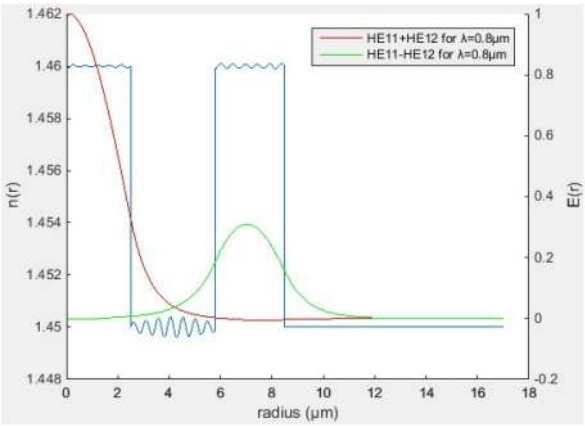

Fig. 7 *Reconstructed coaxial couple RI profile using the modal fields of the field in Fig. 6, using (16)*

calculate the reconstructed RI based on the desired fixed electric field. Then, for every reconstructed RI, we repeatedly calculate the propagation constant β (calculated value) until the arbitrary β_{ini} value converges to the required exact modal β value.

4 Design of coaxial couplers

We apply the methods described in the previous sections in a new way to synthesise waveguides behaving as coaxial couplers. A coaxial coupler operates in a manner that the core light energy is

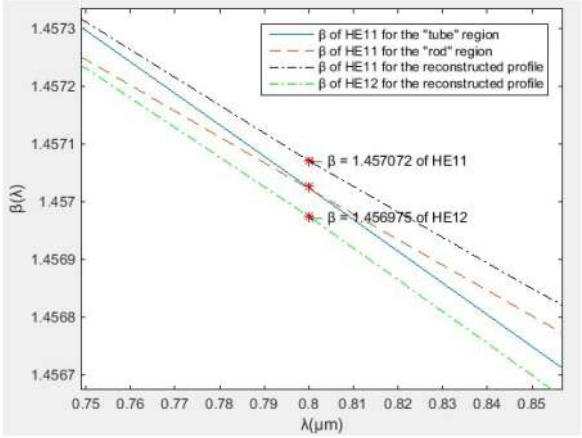

Fig. 8 *Dispersion characteristic of the 'rod', 'tube' and coaxial waveguides. Phase matching is shown at $\lambda = 0.8\,\mu$m, where the dispersion lines 'cross' the 'rod' and 'tube' phase matching occurs*

coupled into the cladding (tube) and the energy oscillates as propagation occurs back and forth across the two regions. We illustrate the technique by designing an optical fibre which supports a 'desired' (hence known) modal field shape both in rod and tube regions. We start the synthesis by using the desired field distribution of the two states of the coupler, i.e. when all the energy is in the core or the alternative when all energy is in the cladding as in Fig. 5. Both coupler state distributions are Bessel functions corresponding on the RI profile of the coupler. The coupling behaviour is also considered using perturbation analysis [2]. We next synthesise the interfering modes of the combined coupler profile (unknown yet).

To reconstruct the single coaxial waveguide supporting this energy transfer, we require first to know the modes of the combined structure. Since the power transfer can be seen as the interference of the HE11 and HE12 modes since it is a cylindrical structure. We recreate the HE11 and HE12 modes by adding and subtracting the two distributions of Fig. 5. The power in every mode can be calculated by the integral $P = \int_0^\infty |E_r(r)|^2 r\,\mathrm{d}r$, and we also ensure the two modes have equal powers.

Assuming Bessel functions for Fig. 5, we can easily synthesise the HE11 and HE12 interfering modes, as seen in Fig. 6. Applying the profile synthesis methods described here, we subsequently find the mode propagation constants and the reconstructed coaxial waveguide modes, which support the desired fields, and finally the derived RI profile of the coaxial coupler, as shown in Fig. 7, which can be seen to be the step-index profile, with which we started, for both core and tube, with minor ripple error. In Fig. 8, we show the dispersion characteristics of the HE11 mode of the constituting rod and tube separate waveguides of the RI profile of Fig. 7, as well as the dispersion of the HE11 and HE12 modes of the total reconstructed coaxial coupler. The phase matching of the 'rod' and 'tube' modes is clear at the wavelength of operation. The propagation constants of the HE11 and HE12 modes of the combined structure appear all in the same figure.

We next proceed to synthesise couplers supporting more complex power distribution in both core and cladding. In the next example, we select Gaussian shapes for the core and cladding field distributions for the two states of the coupler (Fig. 9) (the straight through and cross-states). We ensure equal powers between the modes as in the previous example.

We use for all subsequent examples the wavelength $\lambda = 1.1\,\mu$m. Furthermore, we introduce the beat length L, a parameter [1], and an important parameter dependent on the coupler properties, defined as

$$L = \frac{2\pi}{\beta_{11} - \beta_{12}} = \frac{\lambda}{\overline{\beta_{11}} - \overline{\beta_{12}}} \tag{19}$$

where β_{11} and β_{12} are the propagation constants, of the two interfering modes, responsible for the coupling process. It is often

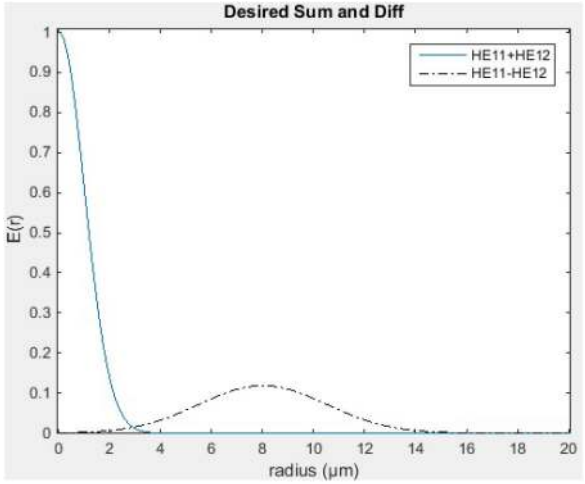

Fig. 9 *Gaussian field both in core and tube: the desired sum and difference of HE11 and HE12 modes versus the radius*

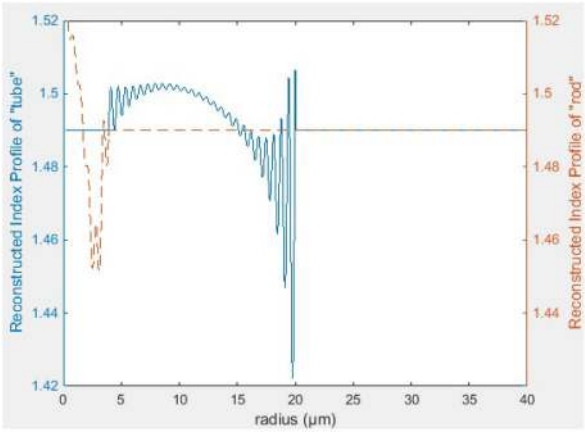

Fig. 10 *'Rod' and 'tube' regions of the reconstructed index profile knowing the HE11 mode*

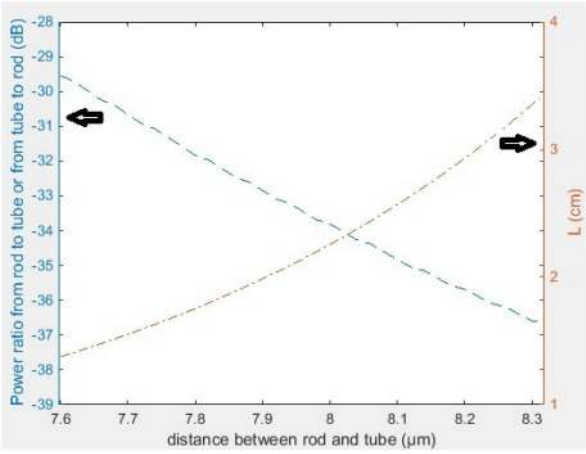

Fig. 11 *The L parameter and the maximum percentage of total power that penetrates in the other region expressed to dB (Gaussian field both in core and tube)*

used as $(\beta_{11} - \beta_{12})/2 = k$ defined as the coupling coefficient. In the following examples, L is plotted versus the distance between the centres of the desired coupler field distributions ('rod-field' and 'tube-field' regions). To change the distance, we move the mean value of the desired 'tube-field' region, to increase the separation.

We select Gaussian field distribution with the straight through state region (core) $\mu = 0$, $\sigma = 1$ and the cross-state (Gaussian ring cladding field) with $\mu = 8$, $\sigma = 2.5$. We adopt the total coupler device radius $a1 = 20$ μm and $n_{\text{cladding}} = 1.49$ for $\lambda = 1.1\,\mu$m. We synthesise the HE11 and HE12 modes, and algorithmically derive

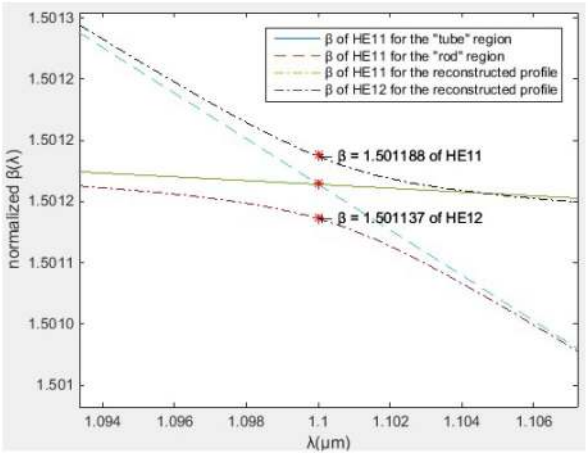

Fig. 12 *Normalised propagation constant β versus λ (Gaussian field both in core and tube)*

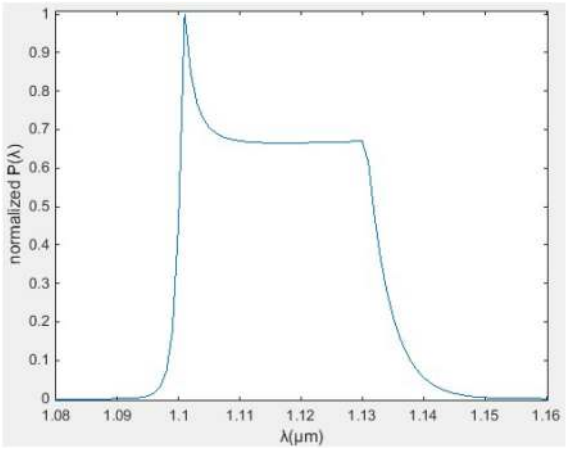

Fig. 13 *Power of HE11 or HE12 versus λ (Gaussian field both in core and tube)*

simultaneously the mode propagation constants and the reconstructed coupler RI profile, as shown in Fig. 10 separating the reconstructed index profile in two parts in the dashed and continuous lines. This split equals to a radius near to the point of the overlap of the two modal fields which we used. Increasing the separation between the desired fields is possible by increasing μ. This effectively increases the beat length L of the coupler as shown by plotting L versus the distance between them in Fig. 11. In the same figure, we also show the coupler crosstalk, which is plotted in dB. The crosstalk levels are excellent, below −28 dB. The index profiles of the 'core' (dotted line) and the 'tube' (solid line) have fundamental modes with a dispersion curve around the design wavelength as shown in Fig. 12. In the same figure, we see the dispersion curves of the interfering modes of the combined structure. Interestingly, the same principles as for the case of step-index guides (Fig. 8) apply here, and we see the phase matching of the core and cladding profiles at the design wavelength, at the point the two curves cross. This is the wavelength where the cross and through coupler states show maximum power transfer. Finally, for this wavelength, we plot in Fig. 13 the wavelength response of the interfering modes, and this is no less than the filtering behaviour of the coaxial coupler. What is fascinating here is the slight asymmetry exhibiting on one side of the operating wavelength compared with the other. This asymmetry is obviously due to the complex index profile used for forcing the desired electric fields. More research is needed here but it is beyond the scope of this paper.

We continue by investigating a fibre coupler, which also supports desired Gaussian field shapes in both regions but the cladding Gaussian ring has been clipped as shown in Fig. 14. The field in the tube is clipped in the region $6.6 < r < 8.6$ also changing the mean value of the Gaussian distribution from $\mu = 8$ to $7.6\,\mu$m.

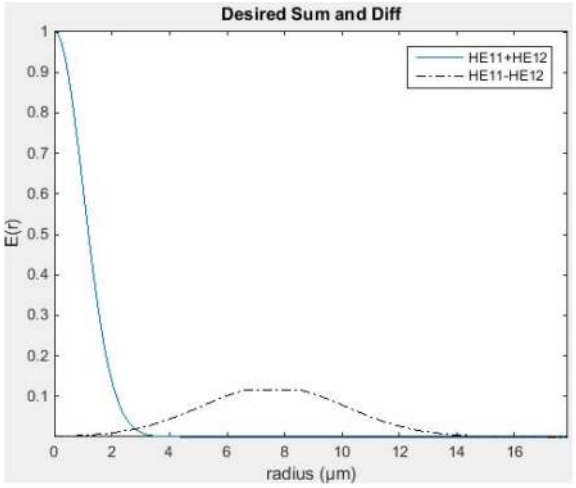

Fig. 14 *Gaussian field in core and clipped Gaussian in the tube: the desired sum and difference of HE11 and HE12 modes versus the radius*

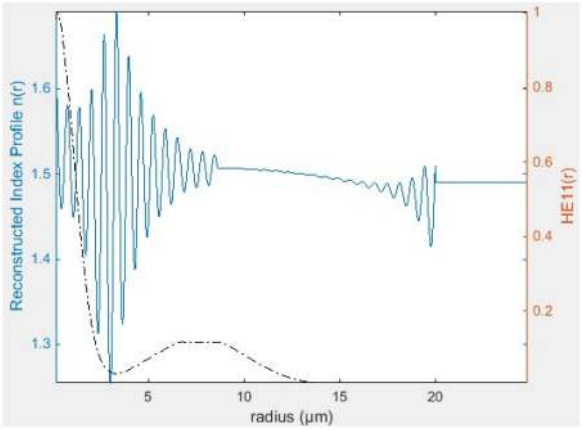

Fig. 15 *Reconstructed RI knowing the HE11 mode*

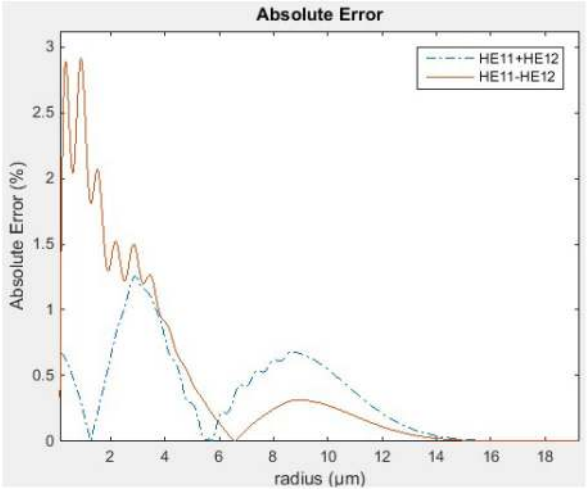

Fig. 16 *Absolute error between desired and produced sum and difference*

Flattened electric-field distributions are useful for high-power laser or amplifier applications. Results of the application of the inverse technique are shown in Fig. 15. The reconstructed fields from this profile add and subtract exactly and shift the optical energy inside and out of the core region as expected. Fig. 16 shows the error between the desired and predicted field distributions, which is <3% in most regions. Fig. 17 shows the coupler crosstalk power of the interfering fields. We can observe this is between −18 and −32 dB. In the same figure, we have plotted the calculated beat length L versus the separation distance between reconstructed 'rod' and 'tube'. As expected, increasing the separation results in longer L.

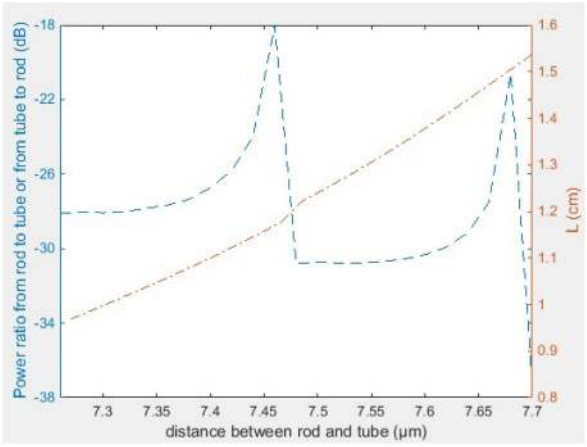

Fig. 17 *The L parameter and the maximum percentage of total power that penetrates in the other region expressed to dB (Gaussian field in the core and clipped Gaussian in the tube)*

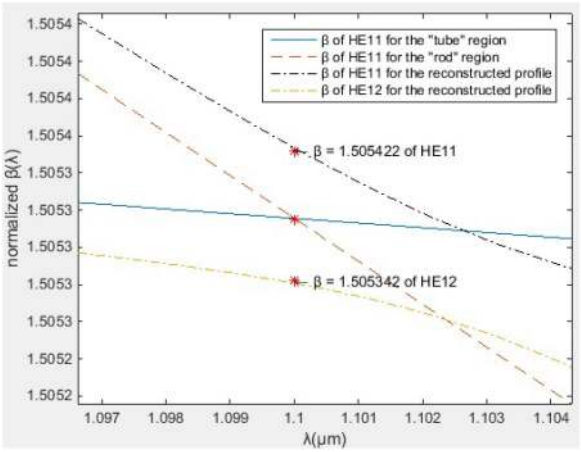

Fig. 18 *Normalised propagation constant β versus λ (Gaussian field in the core and clipped Gaussian in the tube)*

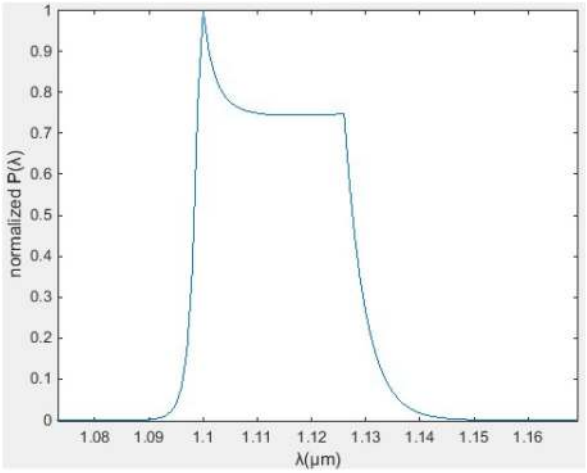

Fig. 19 *Power of HE11 or HE12 versus λ (Gaussian field both in core and tube)*

Fig. 18 shows the dispersion of the propagation modes of the whole structure, and we also show the reconstructed dispersion of the 'core' and 'tube' cladding regions separately. Phase matching again is observed at a wavelength of 1.1 μm. Fig. 19 shows the wavelength response of this coupler, showing complete coupling at the wavelength 1.1 μm.

As a final example, we design an optical fibre with a triangular field profile in the 'rod' region up to radius 5.65 μm, and for larger radius decays exponentially. In the 'tube' region, the field is Gaussian shape with $\mu = 11.8\,\mu$m, $\sigma = 2.2\,\mu$m and clipped between

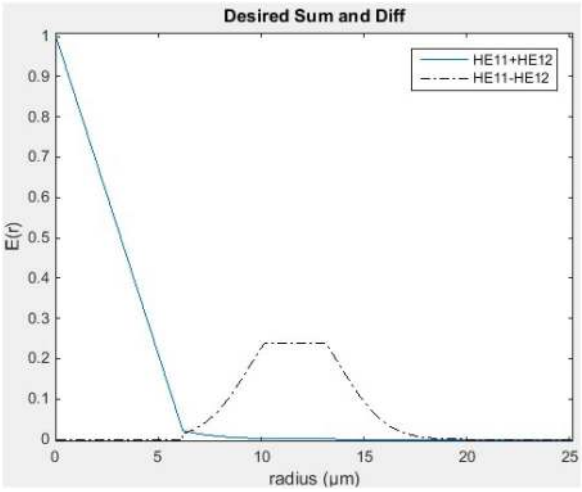

Fig. 20 *Triangular field in core and clipped Gaussian in the tube: the desired sum and difference of HE11 and HE12 modes versus the radius*

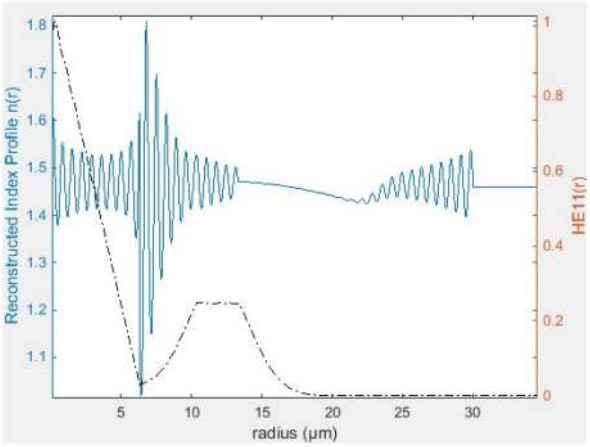

Fig. 21 *Reconstructed RI knowing the HE11 mode*

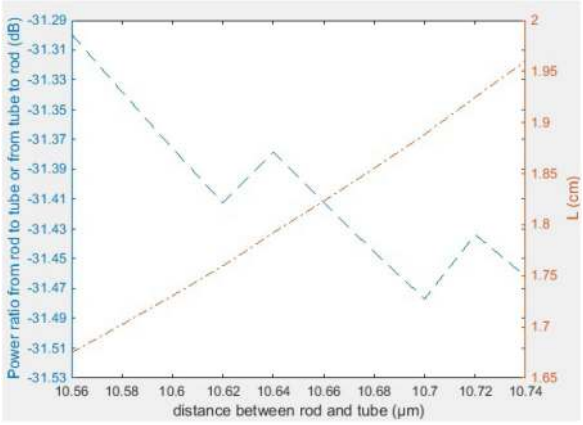

Fig. 22 *The L parameter and the maximum percentage of total power that penetrates in the other region expressed to dB (Triangular field in the core and clipped Gaussian in the tube)*

$10.3 < r < 13.2\,\mu$m, as shown in Fig. 20. We also assume core radius $a1 = 30$ μm and $n_{\text{cladding}} = 1.38$ for $\lambda = 1.1\,\mu$m.

Using those field profiles, we add and subtract them and using our algorithm reconstructs the RI profile supporting the fields as shown in Fig. 21. Fig. 22 shows the crosstalk of the coupler and the beat length L when we modify the gap distance between rod and tube waveguides, and this shows excellent crosstalk <−30 dB possible. Fig. 23 shows the dispersion of the propagation modes of the whole profile structure, and we also show the separate reconstructed dispersion of the fundamental modes of the core and

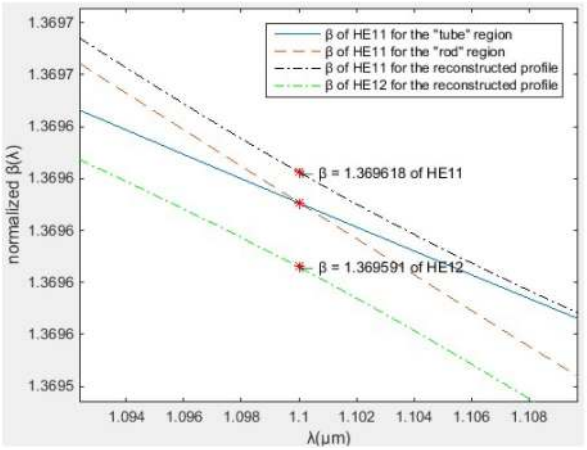

Fig. 23 *Normalised propagation constant β versus λ (Triangular field in the core and clipped Gaussian in the tube)*

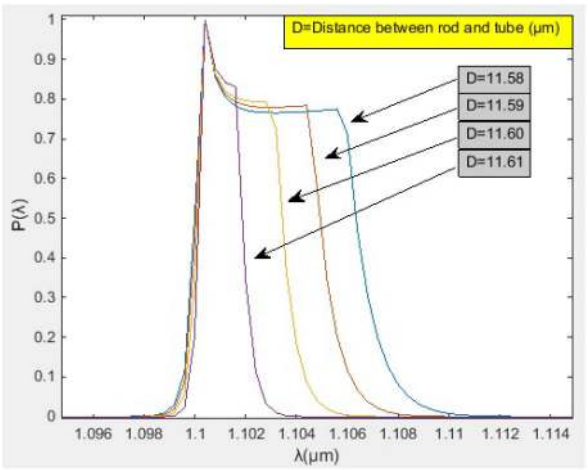

Fig. 24 *Power versus λ and D (the distance between the centres of 'rod-field' and 'tube-field' regions)*

cladding regions. Phase matching again is observed at a wavelength of 1.1 μm.

Fig. 24 shows the variation of the wavelength response of the coupler as we increase the separation between 'rod' and 'tube'. The separation is increased by increasing μ of the Gaussian field. We observe the narrowing of the filtering response of this coupler with increasing the separation of the fields. Finally, this gives insights for the use of such reconstructions as filter designs with designed electric-field distributions different from the usual Bessel functions.

5 Discussion

We have demonstrated the synthesis of several coaxial coupler RI profiles exhibiting unusual arbitrary modal electric fields using the T–L method. However, the presence of an error ripple of the order of 0.02% in index profile of Fig. 7 is inevitable due to the algorithmic procedure. Owing to recursive formulas of (7) and (17), an unexpected small error (due to the accuracy of the calculations) could be accumulated to the next layers. The reconstructions of the RI in Figs. 10, 15 and 21 are effectively coaxial grating structures. The biggest amplitude oscillations are located near sharp changes in the electric fields as expected, because the technique is trying to accommodate these changes, creating large transverse radial index oscillations. The ripple far away into the cladding could be ignored due to the fact the electric field is already too small and decayed and the ripple appears due to the electric-field truncation.

As far as the coupler construction is concerned, it depends on the frequency and amplitude of the grating oscillations. We have placed no limits on those gratings at this stage of study to show the principle of the designs. In practise, someone could consider limits

on those index oscillations to take into account manufacturing constraints.

In Fig. 24, we show the possibility of designing narrowband filters. One approach is by increasing the separation between rod and tube regions. However, this study area, as well as the use of a coupler synthesis as a sensor by varying the RI (for example, the $n3$ RI of Fig. 1) around the coupler is interesting, promising and important and will be a future research topic.

6 Conclusion

In conclusion, we have extended the T–L technique of cylindrical waveguides and presented an exact and efficient algorithm for designing optical fibre couplers of arbitrary modal electric-field distributions. Our purpose was to design a fibre optic device with two pre-selected mode fields such that the beating of those two fields transfers all the optical power in one or the other part of the optical fibre.

By using this method, we have showed by many examples that this is feasible through a choice of the appropriate values for the core radius and cladding RI. We expect T–L technique to be useful for designing optic, temperature or pressure, high-power sensors or biosensors but mostly optic filters.

7 References

[1] Marcuse, D.: '*Light transmission optics*' (Van Nostrand Reinhold, New York, 1972), pp. 407–431

[2] Boucouvalas, A.C.: 'Coaxial optical fiber coupling', *J. Lightwave Technol.*, 1985, **3**, (5), pp. 1151–1158

[3] Xiang, W., Guo, H., Chen, N., *et al.*: 'Cladding mode resonance based fiber for temperature measurement'. China–Japan Joint Microwave Conf., Shanghai, 2008, pp. 571–573

[4] Lu, J., Chen, Z., Pang, F., *et al.*: 'Theoretical analysis of fiber-optic evanescent wave sensors'. China-Japan Joint Microwave Conf., Shanghai, 2008, pp. 583–587

[5] Rosli, M.A.A., Arasu, P.T., Lim, H.N., *et al.*: 'Dynamic response of tapered optical fiber coated with graphene oxide for detecting aqueous ethanol'. Photonics (ICP) IEEE Sixth Int. Conf., Kuching City of Sarawak, Malaysia, 2016, pp. 1–3

[6] Zhang, Q., Song, Y., Zeng, X., *et al.*: 'Fiber mode adapter based on double-cladding fibre for multimode fibre access networks'. 17th Opto-Electronics and Communications Conf., Busan, 2012, pp. 809–810

[7] Boucouvalas, A.C., Georgiou, G.: 'Biconical taper coaxial coupler filters', *Electronic Lett.*, 1985, **21**, (20), pp. 1033–1034

[8] Boucouvalas, A.C., Georgiou, G.: 'External refractive index response of tapered coaxial couplers', *Opt. Lett.*, 1986, **11**, (4), pp. 257–259

[9] Boucouvalas, A.C., Georgiou, G.: 'Tapering of single mode optical fibres', *IEE Proc. J. Optoelectronics.*, 1986, **13**, (6), pp. 385–392

[10] Boucouvalas, A.C., Georgiou, G.: 'Tapered Coaxial Coupler Sensors'. OFS 86, Tokyo, Japan, 7–9 October 1986, pp. PD-2-1–PD-2-5

[11] Boucouvalas, A.C., Qian, X.: 'Optical Fiber Refractive Index Profile Synthesis from Near Field'. IEEE Globecom 2003-Optical Networking and Systems., 2003, pp. 2669–2673

[12] Papageorgiou, C.D., Boucouvalas, A.C.: 'Computation of Mode Propagation Constants and Cut-off Frequencies of Optical Planar Layers Using the Resonance Technique', *Optica Acta.*, 1984, **31**, (5), pp. 555–562

[13] Boucouvalas, A.C., Thraskias, C.A.: 'Accurate Optical Fiber Refractive Index Reconstruction from Near Field', *UbiCC J. CSNDSP.*, 2008, **4**, (5)

[14] Thraskias, C.A., Boucouvalas, A.C.: 'Design of arbitrary modal electric field in planar waveguides', *IET Optoelectronics.*, 2015, **9**, (6), pp. 294–299